Design of quasi-phasematching gratings via convex optimization

C. R. Phillips,[1,2,*] **L. Gallmann,**[2] **and M. M. Fejer**[1]

[1]*Edward L. Ginzton Laboratory, Stanford University, Stanford, California 94305,USA*
[2]*Department of Physics, Institute of Quantum Electronics, ETH Zurich, 8093 Zurich, Switzerland*
[*]*cphillips@phys.ethz.ch*

Abstract: We propose a new approach to quasi-phasematching (QPM) design based on convex optimization. We show that with this approach, globally optimum solutions to several important QPM design problems can be determined. The optimization framework is highly versatile, enabling the user to trade-off different objectives and constraints according to the particular application. The convex problems presented consist of simple objective and constraint functions involving a few thousand variables, and can therefore be solved quite straightforwardly. We consider three examples: (1) synthesis of a target pulse profile via difference frequency generation (DFG) from two ultrashort input pulses, (2) the design of a custom DFG transfer function, and (3) a new approach enabling the suppression of spectral gain narrowing in chirped-QPM-based optical parametric chirped pulse amplification (OPCPA). These examples illustrate the power and versatility of convex optimization in the context of QPM devices.

OCIS codes: (190.4360) Nonlinear optics, devices; (230.7405) Wavelength conversion devices; (190.4970) Parametric oscillators and amplifiers; (320.7080) Ultrafast devices.

References and links

1. M. Charbonneau-Lefort, B. Afeyan, and M. M. Fejer, "Optical parametric amplifiers using chirped quasi-phase-matching gratings I: practical design formulas," J. Opt. Soc. Am. B **25**, 463–480 (2008).
2. L. Gallmann, G. Steinmeyer, U. Keller, G. Imeshev, M. M. Fejer, and J. Meyn, "Generation of sub-6-fs blue pulses by frequency doubling with quasi-phase-matching gratings," Opt. Lett. **26**, 614–616 (2001).
3. G. Imeshev, A. Galvanauskas, D. Harter, M. A. Arbore, M. Proctor, and M. M. Fejer, "Engineerable femtosecond pulse shaping by second-harmonic generation with fourier synthetic quasi-phase-matching gratings," Opt. Lett. **23**, 864–866 (1998).
4. G. Imeshev, M. A. Arbore, S. Kasriel, and M. M. Fejer, "Pulse shaping and compression by second-harmonic generation with quasi-phase-matching gratings in the presence of arbitrary dispersion," J. Opt. Soc. Am. B **17**, 1420–1437 (2000).
5. M. Charbonneau-Lefort, M. M. Fejer, and B. Afeyan, "Tandem chirped quasi-phase-matching grating optical parametric amplifier design for simultaneous group delay and gain control," Opt. Lett. **30**, 634–636 (2005).
6. H. Suchowski, V. Prabhudesai, D. Oron, A. Arie, and Y. Silberberg, "Robust adiabatic sum frequencyconversion," Opt. Express **17**, 12731–12740 (2009).
7. C. R. Phillips and M. M. Fejer, "Efficiency and phase of optical parametric amplification in chirped quasi-phase-matched gratings," Opt. Lett. **35**, 3093–3095 (2010).
8. C. R. Phillips and M. M. Fejer, "Adiabatic optical parametric oscillators: steady-state and dynamical behavior," Opt. Express **20**, 2466–2482 (2012).
9. J. Huang, X. P. Xie, C. Langrock, R. V. Roussev, D. S. Hum, and M. M. Fejer, "Amplitude modulation and apodization of quasi-phase-matched interactions," Opt. Lett. **31**, 604–606 (2006).
10. S. Zhu, Y. Zhu, and N. Ming, "Quasi-phase-matched third-harmonic generation in a quasi-periodic optical superlattice," Science **278**, 843–846 (1997).

#183035 - $15.00 USD Received 8 Jan 2013; revised 1 Mar 2013; accepted 1 Mar 2013; published 16 Apr 2013

11. K. Fradkin-Kashi and A. Arie, "Multiple-wavelength quasi-phase-matched nonlinear interactions," IEEE J. Quant. Electron. **35**, 1649–1656 (1999).
12. K. Fradkin-Kashi, A. Arie, P. Urenski, and G. Rosenman, "Multiple nonlinear optical interactions with arbitrary wave vector differences," Phys. Rev. Lett. **88**, 023903–023906 (2001).
13. M. Asobe, O. Tadanaga, H. Miyazawa, Y. Nishida, and H. Suzuki, "Multiple quasi-phase-matched device using continuous phase modulation of $\chi^{(2)}$ grating and its application to variable wavelength conversion," IEEE J. Quant. Electron. **41**, 1540–1547 (2005).
14. G. Porat, Y. Silberberg, A. Arie, and H. Suchowski, "Two photon frequency conversion," Opt. Express **20**, 3613–3619 (2012).
15. G. Imeshev, M. M. Fejer, A. Galvanauskas, and D. Harter, "Pulse shaping by difference-frequency mixing with quasi-phase-matching gratings," J. Opt. Soc. Am. B **18**, 534–539 (2001).
16. U. Sapaev and D. Reid, "General second-harmonic pulse shaping in grating-engineered quasi-phase-matched nonlinear crystals," Opt. Express **13**, 3264–3276 (2005).
17. M. Conforti, F. Baronio, and C. D. Angelis, "From femtosecond infrared to picosecond visible pulses: temporal shaping with high-efficiency conversion," Opt. Lett. **32**, 1779–1781 (2007).
18. Ł. Kornaszewski, M. Kohler, U. K. Sapaev, and D. T. Reid, "Designer femtosecond pulse shaping using grating-engineered quasi-phase-matching in lithium niobate," Opt. Lett. **33**, 378–380 (2008).
19. M. A. Albota and F. C. Wong, "Efficient single-photon counting at 1.55 μm by means of frequency upconversion," Opt. Lett. **29**, 1449–1451 (2004).
20. J. S. Pelc, L. Ma, C. R. Phillips, Q. Zhang, C. Langrock, O. Slattery, X. Tang, and M. M. Fejer, "Long-wavelength-pumped upconversion single-photon detector at 1550 nm: performance and noise analysis," Opt. Express **19**, 21445–21456 (2011).
21. J. S. Pelc, Q. Zhang, C. R. Phillips, L. Yu, Y. Yamamoto, and M. M. Fejer, "Cascaded frequency upconversion for high-speed single-photon detection at 1550 nm," Opt. Lett. **37**, 476–478 (2012).
22. T. Fuji, J. Rauschenberger, A. Apolonski, V. S. Yakovlev, G. Tempea, T. Udem, C. Gohle, T. W. Haensch, W. Lehnert, M. Scherer, and F. Krausz, "Monolithic carrier-envelope phase-stabilization scheme," Opt. Lett. **30**, 332–334 (2005).
23. C. Langrock, M. M. Fejer, I. Hartl, and M. E. Fermann, "Generation of octave-spanning spectra inside reverse-proton-exchanged periodically poled lithium niobate waveguides," Opt. Lett. **32**, 2478–2480 (2007).
24. C. R. Phillips, C. Langrock, J. S. Pelc, M. M. Fejer, J. Jiang, M. E. Fermann, and I. Hartl, "Supercontinuum generation in quasi-phase-matched $LiNbO_3$ waveguide pumped by a Tm-doped fiber laser system," Opt. Lett. **36**, 3912–3914 (2011).
25. C. R. Phillips, C. Langrock, J. S. Pelc, M. M. Fejer, I. Hartl, and M. E. Fermann, "Supercontinuum generation in quasi-phasematched waveguides," Opt. Express **19**, 18754–18773 (2011).
26. X. Liu, L. Qian, and F. Wise, "High-energy pulse compression by use of negative phase shifts produced by the cascade $\chi^{(2)} : \chi^{(2)}$ nonlinearity," Opt. Lett. **24**, 1777–1779 (1999).
27. J. Moses and F. W. Wise, "Soliton compression in quadratic media: high-energy few-cycle pulses with a frequency-doubling crystal," Opt. Lett. **31**, 1881–1883 (2006).
28. M. Baudrier-Raybaut, R. Haidar, P. Kupecek, P. Lemasson, and E. Rosencher, "Random quasi-phase-matching in bulk polycrystalline isotropic nonlinear materials," Nature **432**, 374–376 (2004).
29. R. Lifshitz, A. Arie, and A. Bahabad, "Photonic quasicrystals for nonlinear optical frequency conversion," Phys. Rev. Lett. **95**, 133901–133904 (2005).
30. C. Canalias and V. Pasiskevicius, "Mirrorless optical parametric oscillator," Nat. Photon. **1**, 459–462 (2007).
31. M. M. Fejer, G. A. Magel, D. H. Jundt, and R. L. Byer, "Quasi-phase-matched second harmonic generation: tuning and tolerances," IEEE J. Quant. Electron. **28**, 2631–2654 (1992).
32. J. S. Pelc, C. R. Phillips, D. Chang, C. Langrock, and M. M. Fejer, "Efficiency pedestal in quasi-phase-matching devices with random duty-cycle errors," Opt. Lett. **36**, 864–866 (2011).
33. C. R. Phillips, J. S. Pelc, and M. M. Fejer, "Parametric processes in quasi-phasematching gratings with random duty cycle errors," J. Opt. Soc. Am. B (to be published).
34. S. P. Boyd and L. Vandenberghe, *Convex Optimization* (Cambridge University, 2004).
35. M. Conforti, F. Baronio, and C. De Angelis, "Nonlinear envelope equation for broadband optical pulses in quadratic media," Phys. Rev. A **81**, 053841–053844 (2010).
36. O. Gayer, Z. Sacks, E. Galun, and A. Arie, "Temperature and wavelength dependent refractive index equations for MgO-doped congruent and stoichiometric $LiNbO_3$," Appl. Phys. B: Lasers Opt. **91**, 343–348 (2008).
37. M. Grant and S. Boyd, *CVX: Matlab Software for Disciplined Convex Programming, version 1.21* (2011).
38. V. J. Hernandez, C. V. Bennett, B. D. Moran, A. D. Drobshoff, D. Chang, C. Langrock, M. M. Fejer, and M. Ibsen, "104 MHz rate single-shot recording with subpicosecond resolution using temporal imaging," Opt. Express **21**, 196–203 (2013).
39. G. Imeshev, M. A. Arbore, M. M. Fejer, A. Galvanauskas, M. Fermann, and D. Harter, "Ultrashort-pulse second-harmonic generation with longitudinally nonuniform quasi-phase-matching gratings: pulse compression and shaping," J. Opt. Soc. Am. B **17**, 304–318 (2000).
40. S. Yang, A. M. Weiner, K. R. Parameswaran, and M. M. Fejer, "Ultrasensitive second-harmonic generation

#183035 - $15.00 USD Received 8 Jan 2013; revised 1 Mar 2013; accepted 1 Mar 2013; published 16 Apr 2013

frequency-resolved optical gating by aperiodically poled $LiNbO_3$ waveguides at 1.5 μm," Opt. Lett. **30**, 2164–2166 (2005).
41. Z. Jiang, D. S. Seo, S. Yang, D. E. Leaird, R. V. Roussev, C. Langrock, M. M. Fejer, and A. M. Weiner, "Four-User, 2.5-Gb/s, spectrally coded OCDMA system demonstration using Low-Power nonlinear processing," J. Lightwave Technol. **23**, 143–158 (2005).
42. G. D. Miller, "Periodically poled lithium niobate: modeling, fabrication, and nonlinear-optical performance," PhD dissertation, Stanford University, Stanford, CA (1998).
43. S. Witte and K. Eikema, "Ultrafast optical parametric Chirped-Pulse amplification," Selected Topics in IEEE J. Quant. Electron. **18**, 296–307 (2012).
44. C. Heese, C. R. Phillips, B. W. Mayer, L. Gallmann, M. M. Fejer, and U. Keller, "75 MW few-cycle mid-infrared pulses from a collinear apodized APPLN-based OPCPA," Opt. Express **20**, 26888–26894 (2012).
45. A. Shirakawa, I. Sakane, M. Takasaka, and T. Kobayashi, "Sub-5-fs visible pulse generation by pulse-front-matched noncollinear optical parametric amplification," Appl. Phys. Lett. **74**, 2268–2270 (1999).
46. T. Fuji, N. Ishii, C. Y. Teisset, X. Gu, T. Metzger, A. Baltuska, N. Forget, D. Kaplan, A. Galvanauskas, and F. Krausz, "Parametric amplification of few-cycle carrier-envelope phase-stable pulses at 2.1 μm," Opt. Lett. **31**, 1103–1105 (2006).
47. Y. Deng, A. Schwarz, H. Fattahi, M. Ueffing, X. Gu, M. Ossiander, T. Metzger, V. Pervak, H. Ishizuki, T. Taira, T. Kobayashi, G. Marcus, F. Krausz, R. Kienberger, and N. Karpowicz, "Carrier-envelope-phase-stable, 1.2 mJ, 1.5 cycle laserpulses at 2.1 μm," Opt. Lett. **37**, 4973–4975 (2012).
48. M. Charbonneau-Lefort, B. Afeyan, and M. M. Fejer, "Competing collinear and noncollinear interactions in chirped quasi-phase-matched optical parametric amplifiers," J. Opt. Soc. Am. B **25**, 1402–1413 (2008).
49. M. Charbonneau-Lefort, B. Afeyan, and M. M. Fejer, "Theory and simulation of gain-guided noncollinear modes in chirped quasi-phase-matched optical parametric amplifiers," J. Opt. Soc. Am. B **27**, 824–841 (2010).
50. C. Heese, C. R. Phillips, L. Gallmann, M. M. Fejer, and U. Keller, "Ultrabroadband, highly flexible amplifier for ultrashort midinfrared laser pulses based on aperiodically poled Mg:$LiNbO_3$," Opt. Lett. **35**, 2340–2342 (2010).
51. C. Heese, C. R. Phillips, L. Gallmann, M. M. Fejer, and U. Keller, "Role of apodization in optical parametric amplifiers based on aperiodic quasi-phasematching gratings," Opt. Express **20**, 18066–18071 (2012).
52. M. N. Rosenbluth, "Parametric instabilities in inhomogeneous media," Phys. Rev. Lett. **29**, 565–567 (1972).
53. C. R. Phillips, C. Langrock, D. Chang, Y. W. Lin, L. Gallmann, and M. M. Fejer, "Apodization of chirped quasi-phsematching devces," submitted to J. Opt. Soc. Am. B.
54. G. D. Boyd, "Parametric interaction of focused gaussian light beams," Journal of Applied Physics **39**, 3597–3639 (1968).
55. J. E. Schaar, "Terahertz sources based on intracavity parametric frequency down-conversion using quasi-phase-matched gallium arsenide," PhD dissertation, Stanford University, Stanford, CA (2009).
56. C. R. Phillips and M. M. Fejer, "Stability of the singly resonant optical parametric oscillator," J. Opt. Soc. Am. B **27**, 2687–2699 (2010).

1. Introduction

Quasi-phasematching (QPM) gratings have received much attention for numerous applications in photonics. An advantage of QPM gratings is that almost arbitrary structures can be obtained by lithographic fabrication techniques. This high degree of design flexibility has enabled a wide variety of QPM devices, including chirped QPM gratings to support broad bandwidths and adiabatic frequency conversion [1–8], phase-modulated gratings to support discrete optical channels [9], Fourier-synthetic gratings to support multiple phasematching processes [10–14], custom pulse generation [2, 15–18], quantum frequency conversion [19–21], supercontinuum generation and pulse compression [22–27], and many other devices [28, 29].

The primary constraints on the QPM grating structures implemented in materials like 180° ferroelectrics are (1) a nonlinear coefficient satisfying $\bar{d}(z) \equiv d(z)/d_0 = \pm 1$, where $d(z)$ and d_0 are the relevant nonlinear coefficients in the grating and in the unperturbed material, respectively, (2) the maximum grating length available (typically based on size of the wafer), and (3) the minimum QPM period (typically around 5 μm in MgO:$LiNbO_3$, although much shorter periods have been implemented [30]).

The $\bar{d} = \pm 1$ constraint inherent in QPM gratings, combined with the fact that thousands of QPM domains are typically present in a single device, means that optimal QPM design of three-wave mixing interactions is challenging, even if one can assume only one envelope (e.g. a generated idler wave) is changing within the device. To overcome this issue, one can work in

#183035 - $15.00 USD Received 8 Jan 2013; revised 1 Mar 2013; accepted 1 Mar 2013; published 16 Apr 2013

the first-order-QPM approximation: the grating is written in terms of an arbitrary but smooth phase function $\phi(z)$ and duty cycle function $D(z)$ as

$$\bar{d}(z) = \mathrm{sgn}\left[\cos(\phi(z)) - \cos(\pi D(z))\right] \tag{1a}$$

$$= (2D(z)-1) + \sum_{\substack{m=-\infty \\ m\neq 0}}^{\infty} \frac{2\sin(\pi m D(z))}{\pi m} \exp(im\phi(z)) \tag{1b}$$

$$\equiv \sum_{m=-\infty}^{\infty} \bar{d}_m(z), \tag{1c}$$

where Eq. (1a) implies $\bar{d} = \pm 1$, and Eq. (1b) follows from Eq. (1a) as an identity. This identity could be derived, for example, by assuming a constant duty cycle D and linear phase $\phi(z)$, expressing the resulting periodic grating as a Fourier series, and then noting the point-wise convergence of that series to Eq. (1a) for arbitrary phase and duty cycle. Equation (1c) defines the Fourier coefficients $\bar{d}_m$, and in particular $\bar{d}_1$, which is given by

$$\bar{d}_1(z) = \frac{2\sin(\pi D(z))}{\pi m} \exp(i\phi(z)). \tag{2}$$

Rather than dealing with $\bar{d}$, terms other than $\bar{d}_1$ and $\bar{d}_{-1}$ are neglected, and $\bar{d} = \pm 1$ is replaced by the constraint $|\bar{d}_{\pm 1}| \leq 2/\pi$ (or, with a constant 50% duty cycle, $|\bar{d}_{\pm 1}| = 2/\pi$) [31]. In this first-order-QPM approach, terms of the nonlinear polarization driving the high-frequency pump wave involve $\bar{d}_{-1}$, while those driving the lower-frequency signal and idler waves involve $\bar{d}_{+1}$ (or vice versa, depending on the envelope convention used). Since $\bar{d}$ is real, $\bar{d}_{-1} = \bar{d}_1^*$. For chirped gratings, it is useful to express the grating phase function $\phi(z)$ in terms of the (continuous) grating k-vector $K_g(z)$,

$$\phi(z) = \int_0^z K_g(z')dz'. \tag{3}$$

The first-order-QPM approach is particularly effective since, in many devices of practical interest, gratings with only a narrow spatial frequency bandwidth (narrow range of K_g), relative to their center or carrier spatial frequency, are required. Even if few-cycle pulses are involved, this narrow-grating-bandwidth condition can still hold very well (as discussed in section 4). For chirped gratings, this condition means that the range of periods required is small compared to the average period; for periodic gratings, it means that many periods are present in the device.

As a result of these and similar narrow-bandwidth conditions, there is typically negligible overlap between the spatial frequency spectra of $\bar{d}_i$ and $\bar{d}_j$ for $i \neq j$, and hence only a single term $\bar{d}_i$ must be considered for a particular nonlinear-optical interaction. It should be noted that this non-overlapping-spectra property may not hold when the grating structure has errors arising from the fabrication process [31–33], or when considering high orders of the grating ($\bar{d}_j$ with $|j| \gg 1$); we do not consider these issues here. The first-order QPM approximation has been utilized extensively in both modeling and design of QPM devices.

In this paper, we develop new approaches for the design of optimal first-order-QPM devices. We show that for quite a broad range of configurations, QPM device design can be solved via convex optimization techniques [34], meaning that globally optimum designs can be determined rapidly and reliably. Furthermore, we significantly extend the QPM transfer function approach for generating target pulse profiles developed in [15]. Previously, this approach involved making severe assumptions on the dispersion of one or more of the input waves (for example, neglecting group velocity mismatch (GVM) or group velocity dispersion (GVD) effects). Here, we show how all orders of dispersion can be accounted for exactly for all of the waves, while also maintaining a convex optimization framework.

#183035 - $15.00 USD Received 8 Jan 2013; revised 1 Mar 2013; accepted 1 Mar 2013; published 16 Apr 2013

We also consider optical parametric chirped pulse amplification (OPCPA), and show how a convex optimization approach can be used to design chirped-QPM OPCPA devices which suppress gain narrowing effects (that is, changes in the gain spectrum due to the use of a pump pulse with a non-uniform temporal profile). Another, complementary benefit of a convex-optimization-based approach is that the infeasibility of design problems can be determined: designs goals (for example, target pulse or gain profiles) which are infeasible can be clearly identified as such.

The paper is arranged as follows. In section 2, we extend the transfer function approach of Ref. [15] to include dispersion to all orders while still maintaining a linear mathematical relationship between the generated wave and the QPM grating profile. In section 3, we use the formalism established in section 2 to solve a number of optimal QPM design problems. In section 4, we consider optical parametric chirped pulse amplification (OPCPA) involving chirped QPM gratings, and show how to suppress spectral gain narrowing via an approximate model of the OPCPA process. Lastly, discussion and conclusions are given in sections 5 and 6, respectively.

2. Coupled wave equations

In this section we develop the well-known coupled-wave equation for difference frequency generation (DFG) into a form suitable for optimization. The approach we develop is completely applicable to other QPM processes involving the generation of a wave from one or more waves which are unperturbed by the nonlinear process, including sum frequency generation (SFG), second-harmonic generation (SHG), and optical rectification (OR) with undepleted pump(s).

2.1. Difference frequency generation

We assume that a signal and pump wave are incident on a QPM grating, and assume a plane-wave interaction. The spatial evolution of the generated idler wave is given by [15],

$$\frac{d\tilde{A}_i(\omega)}{dz} = -i\bar{d}(z)\kappa_i(\omega)\int_0^\infty \tilde{A}_s^*(\omega')\tilde{A}_p(\omega+\omega')\exp(-i\Delta k(\omega,\omega')z)\frac{d\omega'}{2\pi}. \tag{4}$$

In this equation, $\kappa_j(\omega) = \omega d_0/(n_j(\omega)c)$, $\bar{d}(z) = d(z)/d_0$ is the normalized nonlinear coefficient discussed in section 1, and $n_j(\omega)$ is the refractive index of wave j. Subscripts i, s, and p represent the idler, signal, and pump, respectively. Tilde denotes a frequency-domain field quantity. The frequency-dependent phase mismatch $\Delta k(\omega,\omega')$ is given by

$$\Delta k(\omega,\omega') = k_p(\omega+\omega') - k_s(\omega') - k_i(\omega), \tag{5}$$

where $k_j(\omega) = n_j(\omega)\omega/c$ is the wavevector associated with the polarization of envelope j, evaluated at frequency ω. The envelopes A_j are defined to contain only positive optical frequency components, and are such that the total electric field satisfies

$$\tilde{E}(z,\omega)u(\omega) = \frac{1}{2}\sum_j \tilde{A}_j(z,\omega)e^{-ik_j(\omega)z} \tag{6a}$$

$$= \frac{1}{2}\sum_j \tilde{B}_j(z,\omega), \tag{6b}$$

where $u(\omega)$ is the Heaviside step function, and Eq. (6b) implicitly defines envelopes B_j. This analytic signal approach leads to the $[0,\infty)$ integration limits in Eq. (4). Note that analytic signals were not used in Ref. [15]: we use them here to make our approach more easily compatible with recent approaches to modeling $\chi^{(2)}$ devices [25, 35]. We define the Fourier transform as

#183035 - $15.00 USD Received 8 Jan 2013; revised 1 Mar 2013; accepted 1 Mar 2013; published 16 Apr 2013

$\tilde{A}(\omega) = \mathscr{F}[A(t)](\omega) = \int_{-\infty}^{\infty} A(t)\exp(-i\omega t)dt$. The envelopes $\tilde{A}_j$ are constant under linear propagation. We assume that the signal and pump waves are unperturbed by the nonlinear process, and hence $\tilde{A}_j(z,\omega) = \tilde{A}_j(0,\omega)$ for $j = s$ and $j = p$. We have also introduced the envelopes B_j: these envelopes are more conventional time-domain envelopes, i.e. envelopes whose inverse Fourier transform directly yields a component of the electric field at position z and time t. For notational simplicity, the definition of these envelopes [Eq. (6b)] does not include a z-dependent phase factor; note that this is in contrast to the "B" envelopes in [15], whose definition involved phases $\exp(-ik_j(\omega_j)z)$ for carrier frequency ω_j of wave j [compare Eqs. (5) and (6) of [15] to Eqs (6a) and (6b) here].

For a DFG process, we assume that there is no input idler. The output idler envelope is found by integrating Eq. (4), which gives

$$\tilde{A}_i(L,\omega) = -i\kappa_i(\omega)\int_0^{\infty} g(\Delta k(\omega,\omega'))\tilde{A}_s^*(\omega')\tilde{A}_p(\omega+\omega')\frac{d\omega'}{2\pi}, \tag{7}$$

where $g(k)$ is the spatial Fourier transform of the normalized nonlinear coefficient,

$$g(k) = \int_{-\infty}^{\infty} \bar{d}(z)e^{-ikz}dz. \tag{8}$$

Note that for a grating of length L, $\bar{d} = 0$ for $z < 0$ and $z > L$.

It is important to consider the linear-optical phase function $k_j(\omega)L$, which is not accounted for explicitly in the envelopes $\tilde{A}_j$ but is included in the envelopes $\tilde{B}_j$. The full input-output relation for the device is thus given by

$$\tilde{B}_i(L,\omega) = -i\kappa_i(\omega)e^{-ik_i(\omega)L}\int_0^{\infty} g(\Delta k(\omega,\omega'))\tilde{A}_s^*(\omega')\tilde{A}_p(\omega+\omega')\frac{d\omega'}{2\pi}, \tag{9}$$

with $\tilde{A}_s(\omega) = \tilde{B}_s(0,\omega)$ and $\tilde{A}_p(\omega) = \tilde{B}_p(0,\omega)$. Equation (9) shows that there is a linear relationship between the spatial Fourier transform of the QPM grating, $g(k)$, and the generated idler wave $\tilde{B}_i(L,\omega)$. To take advantage of this linearity, in subsection 2.2 we express Eq. (9) as a linear system.

2.2. *General matrix formulation of DFG*

To develop a QPM design procedure, we discretize Eq. (9) using an output frequency grid for the idler and a spatial frequency grid for the QPM grating. We define vector $\mathbf{g} = [g(k_1),...,g(k_N)]^T$, i.e. $g(k)$ evaluated on the spatial frequency grid. Similarly, we define an idler vector $\mathbf{B}_\omega = [\tilde{B}_i(L,\omega_1),...,\tilde{B}_i(L,\omega_N)]$ evaluated on its frequency grid (where subscript ω is used here to indicate that $\mathbf{B}_\omega$ represents envelope B_i in the frequency domain). Over the range of the spatial frequency grid, $g(k)$ can be approximated as a linear function of $\mathbf{g}$:

$$g(k) = \mathbf{v}(k)^T\mathbf{g}, \tag{10}$$

where the vector $\mathbf{v}(k)$ is related to the chosen type of interpolation (e.g. piecewise linear). Substituting Eq. (10) into Eq. (9), the components $\tilde{B}_i(L,\omega_n)$ of the idler vector are given by

$$\tilde{B}_i(L,\omega_n) = \left[-i\kappa_i(\omega_n)e^{-ik_i(\omega_n)L}\int_0^{\infty} \mathbf{v}(\Delta k(\omega_n,\omega'))^T\tilde{A}_s^*(\omega')\tilde{A}_p(\omega_n+\omega')\frac{d\omega'}{2\pi}\right]\mathbf{g}, \tag{11}$$

This equation can be re-written into matrix form:

$$\mathbf{B}_\omega = \mathbf{T}\mathbf{g}, \tag{12}$$

#183035 - $15.00 USD Received 8 Jan 2013; revised 1 Mar 2013; accepted 1 Mar 2013; published 16 Apr 2013

where the matrix elements of the DFG coupling matrix **T** correspond to the terms in square brackets in Eq. (11). Equation (12) is the starting point of our optimization procedure. If the electric field profiles of the input pulses and the frequency-dependent phase mismatch are all known, **T** can be evaluated; in an optimization procedure, **T** only needs to be evaluated once, before starting the optimization algorithm. Note that while Δk can in some cases be well-approximated over the bandwidths of interest by a low-order polynomial in its frequency arguments, we have maintained its full functional form.

2.3. *Form of the DFG coupling matrix*

In this subsection, we show examples of the DFG coupling matrix **T**. The form of **T** is the main factor that determines which pulse designs are possible. Its structure originates from the functional forms of the phase mismatch and the nonlinear polarization. If the pump is narrow-bandwidth, then for each output idler frequency there is only a small range of signal frequencies that are able to contribute. There is thus a correspondingly small range of spatial frequencies which contribute, governed by the excursions of Δk over this frequency range.

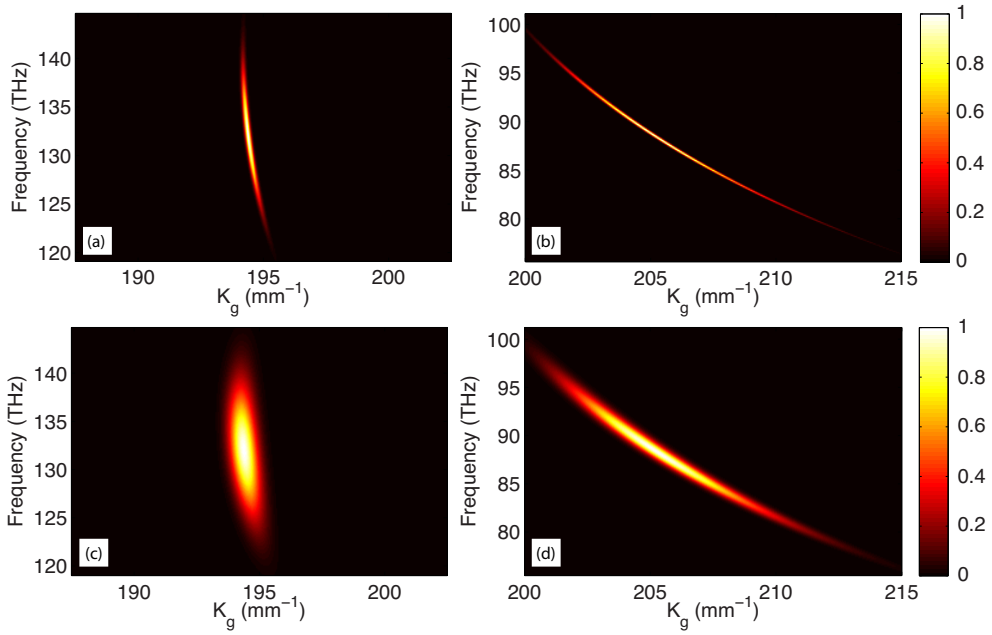

Fig. 1. Magnitude of the DFG coupling matrix **T** for several experimental configurations. (a) Narrow-bandwdith pump, nearly group velocity matched signal and idler waves, (b) narrow-bandwidth pump, group velocity mismatched signal and idler, (c) broadband pump, nearly group velocity matched signal and idler, (d) broadband pump and signal, with group velocity mismatch. $|\mathbf{T}|$ is plotted in each case, and the parameters are given in the text.

The range of spatial frequency components that contribute also depends on the type of interaction involved. If under the same narrow-bandwidth pump approximation there is no GVM between the signal and idler waves at their center frequencies, then **T** will depend mostly on group velocity dispersion and will have a "crescent" like shape. This shape in fact persists even in the presence of GVM, but is tilted in $\omega - K_g$ space. These general properties are illustrated in Fig. 1. The parameters for the figure are as follows. The pump center wavelength is 1064 nm. The signal center wavelength is either 1550 nm [Figs. 1(a) and 1(c)] or 2000 nm [Figs. 1(b) and

#183035 - $15.00 USD Received 8 Jan 2013; revised 1 Mar 2013; accepted 1 Mar 2013; published 16 Apr 2013

1(d)]. Both the signal and pump pulses are Gaussian with no chirp. The signal $1/e^2$ duration is 40 fs, while the pump $1/e^2$ duration is either 2 ps [for Figs. 1(a) and 1(b)] or 200 fs [Figs. 1(c) and 1(d)]. We assume a MgO:$LiNbO_3$ crystal at room temperature [36], and an all-e-wave interaction.

We use piecewise-linear interpolation in Eq. (10) to perform the integrals in Eq. (11). Note that each term can involve integrating over more than one interval in ω' (in particular, this is necessary if $\Delta k(\omega,\omega')$ passes through a minimum or maximum with respect to ω').

As can be seen from Figs. 1(c) and 1(d), when both of the input waves are broad bandwidth, the matrix is smeared out with respect to spatial frequency: a large range of spatial frequencies contribute to each spectral component, and any given spatial frequency drives a wide range of spectral components. For this reason, imposing fine spectral features on the output wave becomes more challenging. In contrast, for a narrowband pump [Figs. 1(a) and 1(b)], the matrix becomes narrower with respect to K_g.

2.4. Transfer function limit

In the limiting case of a cw pump wave but broadband signal and idler waves (or alternatively a cw signal and broadband pump), the nonlinear polarization driving the idler has only a single phase mismatch at each frequency. Mathematically, for a cw pump of frequency ω_p, we have $A_p(\omega) = 2\pi A_{p0}\delta(\omega-\omega_p)$. Therefore, Eq. (9) becomes

$$\begin{aligned}\frac{B_i(L,\omega)}{A_s^*(\omega_p-\omega)} &= -i\kappa_i(\omega)e^{-ik_i(\omega)L}A_{p0}g(\Delta k(\omega,\omega_p-\omega)),\\ &\equiv H(\omega)\end{aligned} \tag{13}$$

where $H(\omega)$ is a transfer function. As discussed in [15], it is not necessary to have a truly cw pump for Eq. (13) to be useful: the pump should simply have a narrow bandwidth compared to the acceptance bandwidths associated with the nonlinear interaction.

Analogously to Eq. (13), the elements of $\mathbf{T}$ are given, in the case of a cw pump, by

$$T_{nm} = -i\kappa_i(\omega_n)e^{-ik_i(\omega)L}A_s^*(\omega_p-\omega_n)A_{p0}v_m(\Delta k(\omega_n,\omega_p-\omega_n)). \tag{14}$$

If the optical frequency and spatial frequency grids coincide, i.e. if for all elements ω_n of the frequency grid, $\Delta k(\omega_n,\omega_p-\omega_n) = k_m$, where k_m is one of the elements of the spatial frequency grid, then $v_m(\Delta k(\omega_n,\omega_p-\omega_n)) = 1$ for such pairs of indices and is equal to zero for all other pairs. In other cases, the general form of $v(\Delta k(\omega_n,\omega_p-\omega_n))$ defined in Eq. (8) can be used. Coinciding grids can be obtained in this transfer function case simply by choosing a non-uniformly spaced spatial frequency grid.

3. Optimal QPM DFG design examples

In this section, we use a convex optimization framework for target pulse generation and transfer function design, based on the formalism developed in section 2. This framework is developed in subsection 3.1. In subsection 3.2, we illustrate the synthesis of target pulse profiles via DFG. In subsection 3.3, we illustrate the design of target QPM DFG transfer functions.

3.1. Optimization framework

The general structure of convex optimization problems is given by Eq. (4.15) of [34]. This mathematical framework supports convex inequality constraints, affine equality constraints, and a convex objective function which is to be minimized. In this section, the variables are the discrete elements of the grating (either on a space or spatial frequency grid), and the generated

#183035 - $15.00 USD Received 8 Jan 2013; revised 1 Mar 2013; accepted 1 Mar 2013; published 16 Apr 2013

idler fields or the QPM DFG transfer function. Related quantities such as derivatives, evaluated by finite differences, can also be included.

Under the first-order QPM approximation, $g(k)$ in Eq. (8) can be accurately evaluated as a spatial Fourier transform of $\bar{d}_{+1}(z)$ rather than $\bar{d}(z)$. Importantly, the equality constraint $|\bar{d}| = 1$ from Eq. (1a) is not affine, while the relaxed constraint $|\bar{d}_1| < 2/\pi$ from Eq. (2) is a convex inequality. Furthermore, as shown above, linear relationships can be established between all of the important variables [for example, Eq. (11)]. Therefore, these quantities can be constrained to have specific values (linear equality constraints), or substituted into convex functions (convex inequality and objective functions). Additionally, $\bar{d}_1$ can typically be resolved with a grid having of order a thousand points, which is convenient for optimization purposes.

Since the QPM grating must have a finite length, we treat the optimization variable as $\bar{d}_1(z)$, expressed on a grid of z points. $\bar{d}_1(z)$ is assumed to be zero outside this grid. $g(k)$ is found by a Fourier transform. The equality constraint $|\bar{d}_1| = 2/\pi$ is not affine (and hence not compatible with our approach), and therefore solutions typically imply a spatially varying QPM duty cycle [see Eq. (2)]. Nonetheless, we can impose the necessary constraint that $|\bar{d}_1| < 2/\pi$. We also show in subsection 3.3 that designs having $|\bar{d}_1| = 2/\pi$ can be obtained by an appropriate choice of objective function. A smooth and slowly-varying $\bar{d}_1(z)$ can be achieved straightforwardly by expressing its spatial derivatives as matrix multiplications and imposing additional constraints. Another possible constraint useful in some situations, but which we do not exploit here, is that particular regions of the grating can be constrained to not deviate substantially from a particular target spatial profile $\bar{d}_T(z)$.

Since $g(k)$ can be obtained from $\bar{d}_1$ by matrix multiplication, similar constraints can be applied to it as well. In particular, $g(k)$ can be constrained to be close to a target spectrum, $|g(k) - g_T(k)| < \varepsilon$ (for some ε). The closeness to this target can be treated as an inequality constraint (fixed ε) or as the optimization variable (minimize ε while satisfying the specified constraints). Since $\tilde{B}_i(\omega)$ and $B_i(t)$ are also obtained by matrix multiplications, the same holds for generating a pulse with a target temporal or spectral profile.

The design examples in the following subsections have been chosen to illustrate some of these properties, but in general many different types of constraints can be imposed onto the grating or the output pulse, beyond those we consider here, in order to suit the problem at hand. To solve the convex optimization problems posed in this paper we use `CVX`, a package for specifying and solving convex programs [37].

The following definitions are used in addition to Eqs. (11) and (13):

$$\mathbf{g} = \mathbf{F_k d} \tag{15a}$$

$$\mathbf{B}_t = \mathbf{F_t B}_\omega \tag{15b}$$

$$\frac{d^n f}{dz^n} \approx \mathbf{D_n f} \tag{15c}$$

where $\mathbf{F_k}$ is a discrete spatial Fourier transform, $\mathbf{F_t}$ is a discrete inverse temporal Fourier transform, $\mathbf{B}_t$ is a discrete approximation to $B_i(L,t)$, $\mathbf{d}$ is a sampled version of $\bar{d}_1(z)$, and $\mathbf{D_n}$ is a square matrix which approximates the relevant n^{th} derivative (e.g. a spatial derivative if applied to $\mathbf{d}$). The l_n norm is denoted $\|.\|_n$, and $|\mathbf{f}|$ denotes the point-wise magnitude of the elements of $\mathbf{f}$.

3.2. Generation of target pulse profiles

In this subsection we show the design of a target temporal pulse profile, denoted $\mathbf{B}_{\text{target}}$. If a particular pulse profile is needed for an experiment, generating that pulse via DFG provides a particularly simple experimental approach, especially if the desired pulse is in a new wavelength

#183035 - $15.00 USD Received 8 Jan 2013; revised 1 Mar 2013; accepted 1 Mar 2013; published 16 Apr 2013

range where pulse synthesis is not convenient, such as the mid-IR. Rather than employ complicated optical arrangements such as pulse shapers, DFG-based pulse shaping can be employed in a purely collinear geometry without spatially or temporally dispersing the input pulses [15]. The approach presented here is a key step forwards in the context of this approach, since it can be used to directly design a finite-length grating which, given known input pulses, yields the target output pulse, without approximating the dispersion of the medium.

Additionally, the optimization algorithm can be used to determine with some confidence if generating a particular pulse is infeasible given the input pulses. It is also possible to test the utility of chirping one of the input pulses. The QPM grating can then be designed according to whichever input chirp profile is convenient (such as propagation through a piece of bulk material); it is even possible to compensate higher order phases entirely by the QPM grating design rather than by complicated dispersion compensation systems [5].

The simplest approach is to treat $\mathbf{d}$ as a complex variable, and minimize $\|\mathbf{B}_t - \mathbf{B}_{\text{target}}\|_2$ with no constraints. However, this approach is unlikely to yield a "clean" grating profile. Instead, we solve the following convex optimization problem:

$$\text{minimize } \|\mathbf{D_2 d}\|_2 \tag{16a}$$

$$\text{subject to:}$$

$$\frac{\|\mathbf{B}_t - \mathbf{B}_{\text{target}}\|_2}{\|\mathbf{B}_{\text{target}}\|_2} \leq \varepsilon \tag{16b}$$

$$|\mathbf{d}| \leq 2/\pi. \tag{16c}$$

where $\mathbf{d}$ is the (complex-valued) optimization variable. Minimizing $\|\mathbf{D_2 d}\|_2$ leads to a grating profile which is as smooth as possible, without the need to specify an explicit upper bound (a suitable value for which might not be known *a priori*). In this problem, ε is chosen according to the tolerable deviations of the pulse from the target. Note that the energy of the target pulse, i.e. $\|B_{\text{target}}\|_2^2$, can be varied in order to obtain a solution whose duty cycle profile is as close to 50% as possible ($|\mathbf{d}| = (2/\pi)\mathbf{1}$). Further details are given in Fig. 2.

The grating length L is determined implicitly by the z grid: while $\mathbf{d}$ can be constrained to equal zero in the outer regions of the grid (or over any region of the grid), there is no computational advantage to doing so. However, if designs involving duty cycle apodization are favorable, then the first and last elements of $\mathbf{d}$ can be constrained to equal zero: this, in combination with the objective function, will favor nonlinear coefficients which are turned on/off smoothly at the edges of the grating. L can be chosen to equal a maximum length (determined for example by fabrication constraints), or estimated based on the dispersion of the crystal.

To illustrate a solution to Eq. (16), we choose as inputs a 500-fs ($1/e^2$) Gaussian pump pulse centered at 1064 nm, and a 25-fs ($1/e^2$) Gaussian signal pulse centered at 1550 nm. We allow for a 10-mm MgO:$LiNbO_3$ grating length, and assume that the pulses are temporally overlapped at the center of the grating. Figure 2 shows an example mid-IR target pulse and corresponding solution to problem (16).

To illustrate the generality of the technique, the target pulse in Fig. 2 was chosen randomly with characteristic temporal features of durations bounded below by the input pulse durations and above by the maximum delays associated with the distance over which the input pulses remain temporally overlapped, and the resulting range of idler group delays. A target pulse satisfying these bounds is calculated by applying Gaussian filters to an initial vector whose elements have random and uniformly distributed real and imaginary parts. We have found that the optimization routine almost always finds a sensible (smooth grating) solution for such random pulses provided that these bounds are imposed. Figure 2 therefore shows that generating arbitrary target pulse profiles is straightforward with our convex optimization approach, and could hence be applied in many waveform synthesis problems.

#183035 - $15.00 USD Received 8 Jan 2013; revised 1 Mar 2013; accepted 1 Mar 2013; published 16 Apr 2013

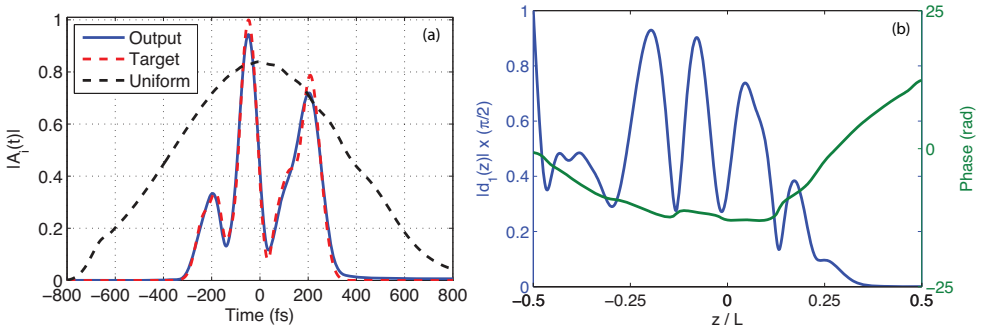

Fig. 2. Example solution to the optimization problem given in Eq. (16). (a) Output (solid blue curve) and target (dashed red curve) amplitude profiles. (b) Corresponding grating profile (amplitude and phase). Rather than specify the energy directly, we normalize the energy U to that of the pulse which would be generated in a grating with a uniform QPM profile, $K_g = \Delta k(\omega_i, \omega_s)$ for carrier frequencies ω_s, ω_p, and $\omega_i = \omega_p - \omega_s$; this energy is denoted U_0. The black dashed line in the figure shows the amplitude profile of a pulse generated by such a grating. The energy of the target pulse in this example is given by $U/U_0 = 0.3$. The $\|\mathbf{B}_t - \mathbf{B}_{\text{target}}\|_2$ and $\|\mathbf{B}_{\text{target}}\|_2$ norms in Eq. (16) are evaluated over a 2-ps temporal window, and $\varepsilon = 0.1$.

3.3. *Design of custom transfer functions*

In this subsection, we next consider the QPM transfer function limit discussed in section 2.4. Such transfer functions can be utilized in various contexts, for example time lens systems [38], pulse compression via SHG [39], pulse characterization [40], telecom applications [41], as well as pulse synthesis [15]. We show the optimal design of a target transfer function with advantageous properties not easily achievable by analytical or local-optimization design approaches. In section 3.2 we showed target waveform synthesis, but did not constrain the QPM duty cycle to be constant. However, constant duty cycle designs are often favorable in terms of QPM fabrication technology [42]. Therefore, for the example presented in this section, we show how a constant 50% duty cycle QPM device can be designed by our approach.

Certain target transfer functions are more compatible with constant-duty-cycle gratings than others. Therefore, to construct an illustrative example, we choose a target transfer function having phase corresponding to the group delays predicted by a simple model for chirped QPM gratings. Specifically, for a smoothly chirped QPM grating with a monotonic $K_g(z)$ profile and a cw (or narrowband) pump wave, the output idler group delay can be estimated as [5]

$$\tau_i(\omega) = \tau_s(\omega_p - \omega) + \frac{z_{pm}(\omega)}{v_{g,s}(\omega_p - \omega)} + \frac{L - z_{pm}(\omega)}{v_{g,i(\omega)}} \tag{17}$$

where $z_{pm}(\omega)$ is the phasematching point, satisfying $\Delta k(\omega, \omega_p - \omega) - K_g(z_{pm}(\omega)) = 0$, with $\Delta k(\omega, \omega')$ defined in Eq. (5). $v_{g,j}(\omega)$ denotes the group velocity of wave j at frequency ω, and L is the crystal length. $\tau_s(\omega)$ is the group delay of the signal at the input of the QPM grating.

As discussed in [5], the idler group delay in Eq. (17) has a relatively simple origin: each spectral component ω travels with the signal before its phasematching point, and hence accumulates delay according to the signal group velocity at the corresponding signal frequency (i.e. $v_{g,s}(\omega_p - \omega)$). However, for the rest of the crystal length after $z_{pm}(\omega)$ (distance $L - z_{pm}(\omega)$), it travels at the idler group velocity $v_{g,i}(\omega)$.

It is possible to use Eq. (17) to construct an ordinary differential equation for the $K_g(z)$ profile which will yield a target idler group delay $\tau_i(\omega)$ (or to determine if a target is not

#183035 - $15.00 USD Received 8 Jan 2013; revised 1 Mar 2013; accepted 1 Mar 2013; published 16 Apr 2013

possible with a monotonically chirped QPM grating). However, since our goal here is to illustrate an optimization method, we take a simpler approach to constructing the target transfer function. We first select a crystal length and a target bandwidth, and then choose a center spatial frequency and constant grating chirp rate sufficient to generate an idler across this bandwidth. We then substitute this $K_g(z)$ profile into Eq. (17) and assume a transform limited input signal ($\tau_s(\omega) = 0$) to determine $\tau_i(\omega)$. $\tau_i(\omega)$ is then integrated to obtain a spectral phase $\phi_i(\omega)$ (since $\tau_i = -\partial\phi_i/\partial\omega$). The target transfer function is then chosen to be $H_T(\omega) = |H_T(\omega)|\exp(i\phi_i(\omega))$, where $|H_T(\omega)| = H_0$ for ω within the chosen idler bandwidth (H_0 constant), and zero otherwise. The target amplitude and phases are shown in Fig. 3.

We wish to obtain a design which is close to the target within the passband ($H_T(\omega) \neq 0$), and whose errors within this region are both small and slowly varying. We give little emphasis in the design to the regions outside the passband, since these regions are much less significant provided that the input spectrum is bandwidth-limited (as is often the case).

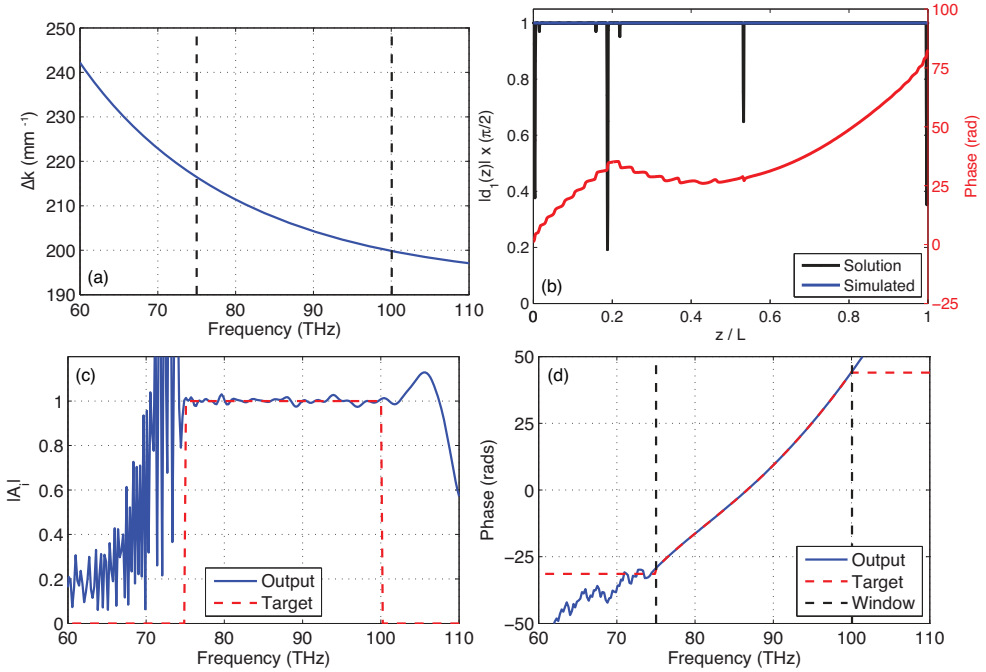

Fig. 3. Example solution to the optimization problem given in Eq. (18). The parameters are given in the text. (a) Phase mismatch $\Delta k(\omega, \omega_p - \omega)$ as a function of idler frequency in THz. Vertical dashed black lines indicate the target passband. (b) Grating profile (amplitude and phase of $d(z)$). The profile returned by the optimization algorithm exhibits a small number of dips in $|d(z)|$ as shown by the black curve. We remove these dips and assume a constant $|d(z)|$ in calculating the transfer function. (c) and (d): Transfer function amplitude and phase.

#183035 - $15.00 USD Received 8 Jan 2013; revised 1 Mar 2013; accepted 1 Mar 2013; published 16 Apr 2013

The optimization problem we solve is given by

$$\text{minimize: } \max(|\mathbf{d}|) \tag{18a}$$

$$\text{subject to:}$$

$$\frac{\|\mathbf{H}[PB]-\mathbf{H}_T[PB]\|_2}{\|\mathbf{H_T}\|_2} \leq \varepsilon_1 \tag{18b}$$

$$|\mathbf{D_1 d}| \leq \lambda_D \tag{18c}$$

$$\left\| \mathbf{D_2} \left(\frac{\mathbf{H}[PB]-\mathbf{H}_T[PB]}{\max(\mathbf{H}_T)} \right) \right\|_1 \leq \varepsilon_2 \frac{\tau_{\text{GVM}}}{\delta\omega} \tag{18d}$$

where $\delta\omega$ is the spacing of the angular optical frequency grid, $[PB]$ denotes the indices corresponding to the passband (the components for which $\mathbf{H}_T \neq 0$), and λ_D is a distance comparable to the average QPM period. $\tau_{\text{GVM}} = |v_{g,s}(\omega_s) - v_{g,i}(\omega_i)|L$ is the group delay accumulated between the signal and idler over the length of the crystal. The parameters ε_1 and ε_2 are small and chosen according to the design goals (described below).

We have chosen the above problem formulation for several reasons. First, the objective function (18a) favors solutions with constant or nearly-constant $|\mathbf{d}|$. Such solutions can be approximated as having constant duty cycle, and are hence easier to fabricate. Constraint (18b) ensures that the transfer function is close to the target. Constraint (18c) prevents $\mathbf{d}$ from varying rapidly over a single QPM period, since such features may not be captured by the actual grating or can result in small QPM domains. Constraint (18d) is chosen to ensure that the deviations of the transfer function from the target are smooth. More specifically: the term $\mathbf{D_2}((\mathbf{H}-\mathbf{H}_T)/\max(\mathbf{H}_T))$ yields a second derivative with respect to angular frequency; taking the 1-norm of the magnitude of this vector and multiplying by $\delta\omega$ corresponds to integration, and hence yields an effective delay. We expect that in a high quality design having slowly-varying deviations from the target transfer function, this 'accumulated' group delay should be much less than the maximum delays supported by GVM within the crystal length, and hence we select a small value for ε_2.

A solution to problem (18) is shown in Fig. 3. We choose a target function with a passband between 1450 nm and 1650 nm, and a cw 1064-nm pump. The corresponding idler passband is from 3000-4000 nm. We assume a 10-mm MgO:$LiNbO_3$ grating at 150 °C. To calculate the group delay in Eq. (17) we assume a linear grating profile given by $K_g(z) = K_{g0} + K_{g1}(z - L/2)$ for $K_{g0} = 208.1$ mm^{-1} and $K_{g1} = 3.3$ mm^{-2}. For the solution shown, we assume $\varepsilon_1 = 0.1$ and $\varepsilon_2 = 10^{-3}$.

Within the passband, the transfer function (TF) amplitude is close to the target and is slowly varying; similarly, the phase shows no visible deviation from the target on the scale shown. This profile comes at the cost of increased ripples outside the passband, since these regions were not constrained at all. Fluctuations in these regions could also be suppressed by adding additional constraints, but at the cost of some performance within the passband.

The modulated grating phase profile [Fig. 3(b)] which yields this result is quite unintuitive, highlighting the importance of having a global optimization framework. By using Eq. (17) to construct an initial $K_g(z)$ profile based on a target group delay spectrum, our method could be applied to a wide variety of transfer function designs. Furthermore, we chose a constant-amplitude target function for illustration purposes. Such a profile is not usually obtained for two reasons: firstly, because ripples on the transfer function are usually partially (but not completely) suppressed by apodization techniques, and secondly because the driving term in Eq. (4) is proportional to the idler optical frequency, which changes substantially over the chosen passband; therefore, part of the phase modulation in the grating arises in order to compensate for this frequency dependence. As such, it is possible to accomodate non-uniform target am-

#183035 - $15.00 USD Received 8 Jan 2013; revised 1 Mar 2013; accepted 1 Mar 2013; published 16 Apr 2013

plitude profiles as well. Therefore, this design approach (and variations thereof) is likely to be applicable to a wide range of optical systems employing QPM gratings.

4. Optimal design of chirped QPM gratings for OPCPA

In this section, we consider optical parametric chirped pulse amplification (OPCPA). OPCPA is a widely-used technique for generating ultrashort, high-energy pulses [43–46]. Typically, a narrow-bandwidth pump wave amplifies the highly chirped, broadband signal and idler pulses. A key consideration is amplification bandwidth. Several schemes have been utilized to obtain broad bandwidths, including noncollinear mixing geometries [45], operation at degeneracy [46], and operation at high gain rates [47]. Another promising approach is the use of chirped QPM gratings [1,5,7,44,48–51]. In this latter case, the gain bandwidth is chosen by designing a crystal with a sufficient spatial frequency bandwidth to amplify all of the spectral components of the signal and idler. Such devices have been studied theoretically [1, 7] and demonstrated experimentally [44, 48, 50, 51].

An important issue in any OPCPA scheme is gain narrowing. That is: the reduction in the gain for spectral components of the chirped signal and idler pulses which are not overlapped (temporally) with the peak of the pump intensity profile. In this section, we build on the theoretical framework of Ref. [1] in order to show how a flat spectral gain profile can be obtained even for a Gaussian pump pulse, thereby suppressing gain narrowing. In subsection 4.1 we determine the frequency-dependent gain for an OPCPA experiment utilizing chirped QPM gratings. In subsection 4.2 we recast this solution into a form suitable for convex optimization. In subsection 4.3, we use this formalism to show how spectral gain narrowing effects can be (optimally) suppressed.

4.1. Approximate form of the signal gain

Assuming an undepleted pump wave, the coupled wave equations governing the evolution of plane-wave signal and idler envelopes are given by

$$\frac{d\tilde{A}_i(\omega)}{dz} = -i\bar{d}(z)\kappa_i(\omega)\int_0^\infty \tilde{A}_s^*(\omega')\tilde{A}_p(\omega+\omega')\exp(-i\Delta k(\omega,\omega')z)\frac{d\omega'}{2\pi}. \tag{19a}$$

$$\frac{d\tilde{A}_s(\omega)}{dz} = -i\bar{d}(z)\kappa_s(\omega)\int_0^\infty \tilde{A}_i^*(\omega')\tilde{A}_p(\omega+\omega')\exp(-i\Delta k(\omega',\omega)z)\frac{d\omega'}{2\pi}. \tag{19b}$$

where the relevant quantities in Eqs. (19a) and (19b) were defined in section 2.1. These equations are a natural extension of Eq. (4), accounting for changes in both the signal and idler waves. We assume that there is no incident idler, which means that we define the signal as the seeded wave, not the higher-frequency wave.

In the case of a cw pump, Eqs. (19a) and (19b) simplify considerably [this assumption yielded Eq. (13) in the case of DFG, for example]. For a sufficiently narrow-bandwidth pump wave and strongly chirped signal and idler waves, the temporal intensity profile of the pump wave can be accounted for approximately while still maintaining the simplicity of the cw-pump case. Consider the group delays $\tau_s(\omega)$ and $\tau_i(\omega)$ associated with spectral components of the signal and idler, respectively. By assuming that group velocity mismatch (GVM) is negligible compared to the duration of the pump pulse given the length of the device, these group delays satisfy, approximately,

$$\tau_i(\omega_p-\omega) \approx \tau_s(\omega) \tag{20}$$

for pump frequency ω_p. Hence mixing between signal frequency ω and idler frequency $\omega_p-\omega$ involves the pump intensity at delay $\tau_s(\omega)$. Assuming a narrow-band (but not cw) pump, Eqs.

#183035 - $15.00 USD Received 8 Jan 2013; revised 1 Mar 2013; accepted 1 Mar 2013; published 16 Apr 2013

(19a) and (19b) can be written as

$$\frac{d\tilde{A}_i(\omega)}{dz} = -i\bar{d}(z)\kappa_i(\omega)A_p(\tau_i(\omega))\tilde{A}_s^*(\omega_p-\omega)e^{-i\Delta k(\omega,\omega_p-\omega)z} \tag{21a}$$

$$\frac{d\tilde{A}_s(\omega)}{dz} = -i\bar{d}(z)\kappa_s(\omega)A_p(\tau_s(\omega))\tilde{A}_i^*(\omega_p-\omega)e^{-i\Delta k(\omega_p-\omega,\omega)z} \tag{21b}$$

Note that these equations could be derived from Eqs. (19a) and (19b) via stationary phase approximations. Note also that Eq. (20) is a useful approximation for calculating the gain spectrum given a narrow-bandwidth pump, but is not sufficient for calculating the group delay and corresponding spectral phase of the idler for subsequent pulse compression [for such problems, Eq. (17) must be used].

The structure of Eqs. (21a) and (21b) implies that each signal frequency $\omega_s+\Omega$ mixes only with idler frequency $\omega_i-\Omega$, where $\omega_i+\omega_s=\omega_p$. Therefore, it is convenient to define frequency-shifted envelopes $\tilde{a}_j(\Omega)=\tilde{A}_j(\omega_j+\Omega)$. We also neglect higher orders of the QPM grating at this stage, so that $\bar{d}\sim\bar{d}_{\pm1}$ [see Eq. (1)]. As mentioned in section 1, for an energy-conserving first-order QPM process, the nonlinear polarization at the pump frequency (which is not included here since we are neglecting pump depletion) involves $\bar{d}_{-1}$ while the nonlinear polarizations for the signal and idler waves involve $\bar{d}_{+1}$. Thus, combining Eq. (20) with Eqs. (21a) and (21b) yields

$$\frac{d\tilde{a}_i(-\Omega)^*}{dz} = +i\bar{d}_1^*(z)\kappa_i(\omega_i-\Omega)A_p^*(\tau_s(\omega_s+\Omega))\tilde{a}_s(\Omega)e^{i\Delta k(\Omega)z} \tag{22a}$$

$$\frac{d\tilde{a}_s(\Omega)}{dz} = -i\bar{d}_1(z)\kappa_s(\omega_s+\Omega)A_p(\tau_s(\omega_s+\Omega))\tilde{a}_i^*(-\Omega)e^{-i\Delta k(\Omega)z} \tag{22b}$$

where the single-frequency-argument phase mismatch is given by

$$\Delta k(\Omega) = k_p(\omega_p) - k_s(\omega_s+\Omega) - k_i(\omega_i-\Omega). \tag{23}$$

Equations (22a) and (22b) have forms analogous to Eqs. (3) and (4) of Ref. [1]. Based on the complex WKB analysis performed in that paper, and Eq. (16) in particular, the signal gain at frequency shift Ω can be approximated, for a chirped QPM grating that has a slow and monotonic chirp profile and constant 50% duty cycle ($|\bar{d}_1|=2/\pi$ within the structure), as

$$G_s(\Omega) \approx \exp\left[2\int_{z_{tp,1}(\Omega)}^{z_{tp,2}(\Omega)}\sqrt{\gamma(\Omega)^2-\left(\frac{\Delta k(\Omega)-K_g(z)}{2}\right)^2}\,dz\right], \tag{24}$$

where $z_{tp,j}(\Omega)$ are frequency-dependent, real-valued turning points: they are the two positions at which the integrand in Eq. (24) is zero. Equation (24) can only be applied for a frequency Ω when both $z_{tp,j}(\Omega)$ are within the structure (and are not too near to an edge). These turning points are introduced in appendix F of [1]. The frequency-dependent coupling coefficient $\gamma(\Omega)$ satisfies

$$\gamma(\Omega)^2 = \left(\frac{2}{\pi}\right)^2 \frac{(\omega_i-\Omega)(\omega_s+\Omega)d_0^2}{n_i(\omega_i-\Omega)n_s(\omega_s+\Omega)c^2}\frac{2}{n_p(\omega_p)\varepsilon_0 c}I_p(\tau_s(\omega_s+\Omega)), \tag{25}$$

where $I_p(t)$ is the pump intensity.

An important result is the gain for a linearly chirped grating ($dK_g/dz=-\partial\Delta k/\partial z$ constant). Integrating Eq. (24) for this case yields the following gain for the signal intensity:

$$\ln(G_s(\Omega)) = 2\pi\Lambda(\Omega), \tag{26}$$

#183035 - $15.00 USD Received 8 Jan 2013; revised 1 Mar 2013; accepted 1 Mar 2013; published 16 Apr 2013

where $\Lambda(\Omega) = \gamma(\Omega)^2/|\partial\Delta k/\partial z|$. Equation (26) corresponds to the Rosenbluth amplification formula [52]. Since $\gamma(\Omega)$ is strongly frequency dependent in an OPCPA system utilizing signal pulses of comparable duration to the pump, high gain across the whole spectrum can only be obtained by over-saturating the peak of the pump; operating in such a regime may be undesirable for many reasons [7].

4.2. Optimization framework

Our goal is to determine a grating chirp profile $K_g(z)$ which yields a target signal gain spectrum while satisfying several constraints. This problem can be put into convex form by a change of variables in Eq. (24). Our main assumption is that $K_g(z)$ is monotonic: this assumption means that the integration variable in Eq. (24) can be changed to K_g instead of z. The limits of integration in this case are the frequency-dependent k-space turning points $K_{tp,j}$, which satisfy $|\Delta k(\Omega) - K_{tp,j}(\Omega)| = 2\gamma(\Omega)$. For spatial frequencies outside the interval $[K_{tp,1}(\Omega), K_{tp,2}(\Omega)]$, the integrand in Eq. (24) is imaginary. Provided that both $K_{tp,j}(\Omega)$ lie within the range of K_g (i.e. provided that the amplification region of a particular spectral component is fully contained within the grating), the integration limits can be extended to cover the entire range of K_g by taking the real part of the integrand (so that the imaginary components outside the turning points do not contribute). We therefore obtain

$$\ln(G_s(\Omega)) \approx \int_{K_i}^{K_f} \Gamma(\Omega, K) z_K(K) dK \tag{27}$$

where $z_K(K_g) = dz/dK_g$ is the reciprocal of the local chirp rate, expressed as a function of spatial frequency. K_i and K_f are the grating k-vectors at the input and output ends of the device, respectively. The local gain rate Γ is given by

$$\Gamma(\Omega, K) = \mathrm{Re}\left[2\sqrt{\gamma(\Omega)^2 - \left(\frac{\Delta k(\Omega) - K}{2}\right)^2}\right]. \tag{28}$$

Analogously to Eq. (24), Eq. (27) is valid for spectral components for which $\Gamma(\Omega, K_i) = \Gamma(\Omega, K_f) = 0$, provided that the chirp rate $(dz/dK_g)^{-1}$ remains sufficiently slow within the $[K_i, K_f]$ interval.

Since Δk and γ are known functions of frequency, values of K_i and K_f can be chosen in order to contain the amplification regions of all the spectral components of interest. Based on Eq. (27), each spectral component Ω is amplified over the interval $K_g \in [\Delta k(\Omega) - 2\gamma(\Omega), \Delta k(\Omega) + 2\gamma(\Omega)]$; within this region, the local signal-idler coupling rate $\gamma(\Omega)$ sufficiently exceeds the local phase mismatch, since $|\Delta k(\Omega) - K_g| < 2\gamma(\Omega)$. If gain is required over a particular spectral range, the (nominal) range of grating k-vectors should thus be extended beyond the range of $\Delta k(\Omega)$ so that the constraint $\Gamma(\Omega, K_i) = \Gamma(\Omega, K_f) = 0$ is met for all Ω of interest. A simple and sufficient condition can be obtained by imposing this constraint while neglecting the frequency dependence of $\gamma(\Omega)$:

$$\begin{aligned} \max([K_i, K_f]) &= K_{\max} + 2\gamma_0 \\ \min([K_i, K_f]) &= K_{\min} - 2\gamma_0 \end{aligned} \tag{29}$$

where $K_{\max} = \max_\Omega(\Delta k(\Omega))$, $K_{\min} = \min_\Omega(\Delta k(\Omega))$, and $\gamma_0 = \max_\Omega(\gamma)$ (the peak signal-idler coupling rate). For a constant chirp rate $\Delta k' = \partial\Delta k/\partial z$, the grating length required to support this range of k-vectors can be written as

$$L = \Lambda_0 \left[\frac{K_{\max} - K_{\min}}{\gamma_0^2} + \frac{4}{\gamma_0}\right] \tag{30}$$

#183035 - $15.00 USD Received 8 Jan 2013; revised 1 Mar 2013; accepted 1 Mar 2013; published 16 Apr 2013

where $\Lambda_0 = \gamma_0^2/|\Delta k'|$; the resulting signal gain is $\ln(G_s) = 2\pi\Lambda_0$ [Eq. (26)]. Equation (30) can be used as a rough estimate for the required grating length. In an optimized device where all spectral components achieve the same gain, the length will usually be longer than predicted by Eq. (30), since $\gamma(\Omega) \leq \gamma_0$.

Equation (27) shows that the gain in dB is linear in the function $z_K(K_g) = dz/dK_g$. For this reason, we will take z_K to be the optimization variable. The nominal grating profile $K_g(z)$ can be constructed from z_K by noting that the position is given, as a function of K_g, by

$$z(K_g) = \int_{K_i}^{K_g} z_K(K)dK, \tag{31}$$

and this function can be inverted to find $K_g(z)$. Note also that since the approximate model of Eq. (27) does not account for gain ripples that arise from the hard edges of the grating, a grating profile determined by an optimization algorithm based on Eq. (27) alone will yield a gain spectrum with strong ripples in amplitude and phase. However, it is possible to append apodization regions to both ends of the device in order to almost completely suppress such ripples [1, 8, 9, 51]. Here, we use apodization techniques for the example shown in section 4.3. In parallel work, we have analyzed the design of such apodization profiles in detail for chirped QPM interactions, including interactions involving high gain or high pump depletion [53].

To formulate an optimization problem for the grating chirp profile, we specify discrete grids for optical frequency Ω, $[\Omega_1, ..., \Omega_N]$, and spatial frequency K_g, $[K_1, ..., K_N]$. We define a matrix $\mathbf{\Gamma}$ as $\Gamma(\Omega, K_g)$ evaluated on these grids, appropriately weighted by the K_g grid spacing. The log of the signal gain $\mathbf{G_s}$ is thus given simply by matrix multiplication:

$$\ln(\mathbf{G_s}) = \mathbf{\Gamma z_K}. \tag{32}$$

For a uniform grid spacing δK, the (nominal) grating length is given by $L = \delta K(\mathbf{1}^T \mathbf{z_K})$. Since the (logarithmic) gain is linear in $\mathbf{z_K}$, it can be readily optimized.

4.3. Suppression of gain narrowing

In order to demonstrate this QPM design technique and its capabilities, in this section we show a specific design example. The goal of this example is to obtain a smooth and flat gain over a broad optical bandwidth while using a signal pulse chirped to fill a large fraction of a Gaussian pump's intensity profile.

We consider an experimental configuration relevant to mid-IR OPCPA using the approach discussed in Refs. [44, 50, 51]. We assume a Gaussian pump pulse with a center wavelength of 1.064 μm, a FWHM duration of 10 ps, and a peak intensity such that $\gamma_0 = \gamma(\Omega = 0) = 3$ mm^{-1}. The Gaussian input signal pulse has center wavelength 3.5 μm, bandwidth supporting a 35-fs FWHM duration, and for simplicity has a purely quadratic spectral phase such that the actual FWHM duration is 3.5 ps. We consider an undepleted-pump example, so the amplified signal intensity is negligible compared with the pump. Note however that due to the properties of adiabatic frequency conversion [6–8], high pump depletion across the pump temporal profile is also possible for the design we present here; we discuss this regime further in subsection 5.2.

We choose a target amplification range spanning the $1/e^2$ signal pulse bandwidth, which corresponds to spectral components between 3.1- and 4.0-μm. In MgO:LiNbO$_3$ at 150 °C, the grating k-vectors phasematching the ends of this spectrum are $K_{\min} = 2.037 \times 10^5$ m^{-1} and $K_{\max} = 2.189 \times 10^5$ m^{-1}. A linear K_g grid is defined with end-points $K_{\min} - 2\gamma_0$ and $K_{\max} + 2\gamma_0$, to ensure that the entire amplification region of each spectral component is contained within the grating [see Eq. (28)]. A frequency-independent target gain of $G_T = \exp(2\pi\Lambda_T)$ with $\Lambda_T = 2.2$ is chosen, which corresponds to approximately 60 dB power gain. For the value of $\gamma_0 = 3$ mm^{-1}

#183035 - $15.00 USD Received 8 Jan 2013; revised 1 Mar 2013; accepted 1 Mar 2013; published 16 Apr 2013

above, a constant chirp rate of $\kappa' = \pm 4.1\ \mathrm{mm}^{-2}$ would be required to obtain $\Lambda_0 = \gamma_0^2/|\kappa'| = \Lambda_T$. With these values, Eq. (30) predicts a grating length of 6 mm.

We solve the following convex optimization problem for variable $\mathbf{z_K}$:

$$\text{minimize } \|\mathbf{D_1 z_K}\|_2^2 \tag{33a}$$

subject to:

$$-\delta G \geq \mathbf{\Gamma z_K} - \ln(G_T) \leq \delta G \tag{33b}$$

$$L \leq L_{\max} \tag{33c}$$

$$\Lambda_{\min} \leq \gamma_0^2 \mathbf{z_K} \leq \Lambda_{\max}, \tag{33d}$$

which is a quadratic program (QP). The chosen objective function ensures smoothness of the solutions. The parameters $\Lambda_{\min} = 1$ and $\Lambda_{\max} = 10$ indicate bounds on the local chirp rate, and are chosen to ensure a sensible solution. In particular, these parameters were selected such that $0 \ll \Lambda_{\min} \leq \Lambda_T \ll \Lambda_{\max}$; as long as these conditions are met, the solution is not too sensitive to these parameters. Note also that the $\Lambda_{\min} > 0$ constraint ensures monotonicity of the z_K and hence $K_g(z)$.

We choose $\delta G = 0.05$, since this tolerance will typically be satisfactory. δG can be made smaller, but eventually the problem may become infeasible. In general, the length $L_{\max}$ can be treated as a parameter: we solve Eq. (33) for a range of choices of $L_{\max}$, numerically simulate the OPCPA process in the resulting grating with the full coupled-wave equations, and select a feasible value of $L_{\max}$ which yields a useful output spectrum from these simulations. For the present example, we chose $L_{\max} = 12$ mm [twice the minimum length indicated by Eq. (30)]. In the solution shown below, both this maximum length inequality (33c) and the chirp rate bounds (33d) are not active, which emphasizes that very little information, and no scanning of $L_{\max}$, is needed in order to arrive at a good solution. Finally, we apply nonlinear-chirp apodization regions to the grating profile returned by the optimization routine [1] [see Fig. 4(a)]. The resulting total length of the grating is $L \approx 9.55$ mm.

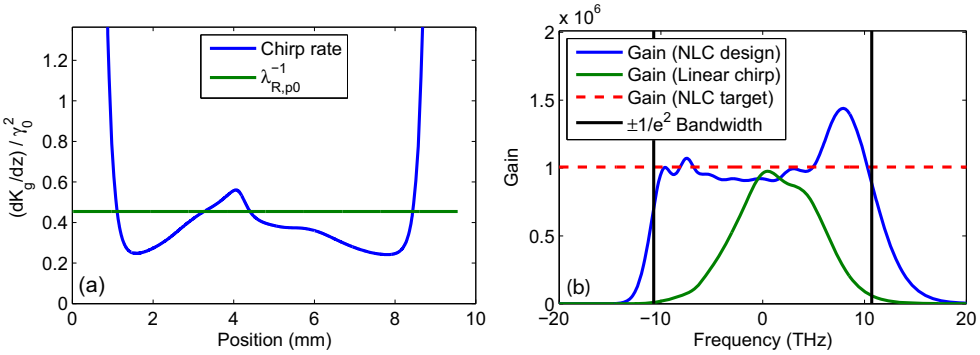

Fig. 4. Nonlinear chirp design example using convex optimization. (a) Optimized chirp rate, normalized to the peak gain coefficient of the pump, γ_0. The horizontal line indicates the constant chirp rate needed for Eq. (26) to yield the target gain spectrum if $\gamma(\Omega) = \gamma_0$. (b) Simulated output spectrum. The spectrum with a nominally linear, apodized chirp profile is shown for comparison.

The optimized grating and simulated gain spectrum is shown in Fig. 4. The simulations are based on Eqs. (19a) and (19b). The dashed horizontal line in Fig. 4(b) indicates the target gain. The actual simulated gain is very close to the target gain; the differences arise due to group velocity mismatch (GVM) and other effects included in the full numerical simulation. The gain

#183035 - $15.00 USD Received 8 Jan 2013; revised 1 Mar 2013; accepted 1 Mar 2013; published 16 Apr 2013

spectrum of a nominally linear, apodized grating design supporting the same OPA bandwidth is shown for comparison, showing pronounced gain narrowing. To quantify the GVM occurring in this example, we denote the rate of temporal walk-off between two waves as $\delta v_{ij} = v_{g,i}^{-1} - v_{g,j}^{-1}$ for waves i and j. For a pump wavelength of 1.064 μm and signal wavelength of 1.45 μm (1.65 μm), the resulting GVM values are given by $\delta v_{si} = -182$ fs/mm (-55 fs/mm); $\delta v_{sp} = -88$ fs/mm (-105 fs/mm); and $\delta v_{ip} = 93$ fs/mm (-49 fs/mm). Thus, given the optimized grating length of 9.55 mm, the range of walk-offs involved is significantly smaller than the duration of the pulses. Nonetheless, GVM still leads to slight modifications in the signal gain spectrum compared with the WKB-predicted spectrum.

A number of other convex formulations of this grating design problem are possible, but Eq. (33) has several advantageous properties. It involves only a small number of free parameters, appropriate values of which can be estimated by inspection. Furthermore, the objective function has two particularly advantageous properties. First, it ensures that $\mathbf{z_K}$ is a good approximation to an underlying smooth variable. Second, recall that this approach relies on the validity of Eq. (24), which in turn relies on having a sufficiently slowly-varying grating chirp: by using smoothness as an objective, we maximize the validity of the approximation upon which the optimization relies.

It is also worth emphasizing that the convex optimization approach allows us to add additional convex constraints as needed. For example, we can easily ensure that the gain spectrum is flat at multiple transverse spatial components of a Gaussian pump beam: for each transverse position $\mathbf{r}$ on the pump, a matrix $\mathbf{\Gamma}(\mathbf{r})$ can be calculated and used to specify additional constraints. Another set of constraints could be obtained by using Eq. (17) to obtain an estimate of the frequency-dependent group delay. It would then be possible to trade off gain narrowing and group delay effects in one or more OPCPA stages.

5. Discussion

5.1. Diffraction and transverse beam effects

In the preceding examples, we have assumed plane-wave interactions. While such assumptions are fully appropriate for waveguide interactions (after performing modal overlap integrals and possibly accounting for higher order spatial modes), in bulk nonlinear interactions transverse beam effects and diffraction can be important [54]. For cases such as OPCPA in which diffraction can be neglected, it is possible to view the nonlinear mixing as a series of interactions at each transverse position on the beams, and hence incorporate these interactions into the optimization problem, as described above.

One heuristic approach in tightly focused cases is to assume Gaussian beam profiles and apply projection integrals as described for example in section 2.4.1 of Ref. [55]. However, for cases such as DFG involving a non-resonant and long-wavelength idler, the generated idler components diverge faster than the nonlinear polarization driving them, and so such approaches may not be very accurate.

A more compelling but also more complicated approach would be to account for diffraction effects exactly within an extension of the optimization framework presented. We showed above how the output field can be expressed as a linear function of the longitudinal spatial frequencies of the QPM grating. However, given the diffracting pump and signal pulsed beam profiles, it would be possible to generalize our analysis to construct a linear system mapping the three-dimensional spatial frequency content of the QPM grating to the optical and transverse spatial frequency components of the output wave. This system could even enable the synthesis of complex spatiotemporal pulses and QPM transfer functions. However, such analysis and optimization of the resulting system are beyond the scope of this paper.

#183035 - $15.00 USD Received 8 Jan 2013; revised 1 Mar 2013; accepted 1 Mar 2013; published 16 Apr 2013

5.2. *Nonlinear interactions with depletion*

In the DFG and OPA examples presented here, we neglected the effects of pump depletion. For QPM transfer functions used for signal processing applications [38], operating in this regime can be useful, since it yields linearity of the output wave with respect to the input wave. In some cases where pump depletion is important, it may be possible to use designs from the linear regime either directly, or as the starting point for general optimization algorithms (for example, by finding a global optimum for the linear case with the methods we have presented, then refining the design via numerical simulations including pump depletion in order to track this optimum as depletion is increased).

For OPCPA pre-amplifiers, the interaction may also typically involve weak pump depletion, so our results are directly relevant to such cases. Furthermore, sufficiently chirped gratings support adiabatic frequency conversion (AFC), which results in a conversion efficiency that monotonically increases with respect to both pump and signal input intensities [6–8]. We have tested via numerical simulations (including pump depletion and dispersion to all orders) that the OPCPA designs shown in section 4 smoothly transition from high gain when the input signal is weak to high pump depletion across most of its temporal profile (and hence across the signal spectrum) when the input signal is strong. Therefore, while our designs assumed an undepleted pump, they are robust against pump depletion effects due to AFC. Nonetheless, strong pump depletion will modify the signal gain spectrum, and should not be ignored.

For SFG and DFG interactions involving depletion of one of the input waves, the corresponding adiabatic frequency conversion processes do not require significant amplification of the signal wave, and therefore approximations of the type used for Eq. (24) may be applicable to this regime as well. For use of such DFG devices inside optical parametric oscillators, we note that stability would be a critical additional consideration [8, 56]. More generally, we note also that linear input/output functions of the type utilized in this paper are not required for convex optimization, and thus a broader class of frequency conversion processes than those considered in this paper may be describable, with suitable approximations, in terms of convex functions.

5.3. *Robustness of the designs*

In terms of robustness, the designs presented share some of the general features of QPM designs. For example, changes in temperature will lead to shifts in phasematching. One factor involved in the temperature sensitivity will be the spatial frequency resolution of the designed grating, which is related to the total grating length. An important point, however, is that sensitivities to experimental parameters can be included inside the optimization algorithm itself. For example, we could take the derivative of the DFG coupling matrix $\mathbf{T}$ defined in Eq. (12) with respect to crystal temperature or delay between the incident pulses, or in general some physical quantity ν, and constrain $\|(\partial\mathbf{T}/\partial\nu)\mathbf{g}\|$ so as to reduce the sensitivity of the output pulses to changes in parameter ν. As such, designs which are robust against changes in one or more system parameters can be achieved in a systematic way.

While such robustness analysis is appropriate for changes in "bulk" parameters, fabricated QPM devices are also subject to an essentially random jitter in the domain sizes and positions. With lithographic poling, the long-range order of the designed structure can be preserved, and only local errors in each of the domain boundaries remain; when such errors are statistically independent of each other, they are called random duty cycle (RDC) errors [31–33]. We have recently studied these errors in detail [33], showing that the resulting pedestal in the spatial frequency spectrum of the QPM grating, which occurs for arbitrary nominal designs, can play a significant role in various experimental configurations. It is therefore important to design experiments which are not excessively sensitive to this pedestal, or, if possible, to improve the fabrication process so as to reduce the size of the RDC errors.

#183035 - $15.00 USD Received 8 Jan 2013; revised 1 Mar 2013; accepted 1 Mar 2013; published 16 Apr 2013

6. Conclusions

In conclusion, we have demonstrated the utility of convex optimization techniques for QPM grating design. This approach can help facilitate new QPM functionalities, including ultrashort pulse synthesis and target OPCPA gain spectra. Furthermore, the approach enables systematic design procedures, by which globally optimum designs can be determined and infeasible design goals can be rejected. The number of variables involved in the discretized problems can be quite large (e.g. several thousand), but these problems can be easily posed and solved with freely available software packages such as `CVX` [37], which make use of fast and reliable interior-point methods (see, for example, chapter 11 of [34]).

Another highly valuable property of the convex optimization approach is that additional constraints can be added straightforwardly, for example to yield a slowly-varying QPM spatial profile, to obtain a flat OPCPA gain spectrum across the spatial profile of a Gaussian pump pulse, or to reduce sensitivity to changes in certain experimental parameters. Practical fabrication constraints such as a maximum grating length can also be included. In developing an optimization framework, we generalized the QPM transfer function formalism, accounting for dispersion to all orders for all the arbitrary-bandwidth interacting waves, while imposing a finite crystal length.

Certain objective functions are particularly useful. The objective function $\max(|\mathbf{d}|)$ tends to result in a solution with $|d(z)| = \max(|\mathbf{d}|)$, which corresponds to a purely phase-modulated grating. Since fabricating QPM gratings with a varying duty cycle is typically quite challenging, this objective function yields a device which can be easily fabricated. Another useful objective function is $\|\mathbf{D_2 d}\|_2$, which yields a smooth grating profile but typically involves some duty cycle modulation, except for certain target pulses or transfer functions.

We have considered representative examples, based on solving quite simple convex optimization problems. As discussed in section 5, it is likely that several other QPM design problems (or relaxations thereof) can also be cast as convex optimization problems. Furthermore, other optical devices such as chirped, dispersion-compensating mirrors, have a similar mathematical structure as the problems we considered here, and may therefore be amenable to the same optimization techniques. We therefore expect these results to be of great use in many aspects of nonlinear optics, custom waveform synthesis, and ultrafast optics.

Acknowledgments

This research was supported by the U.S. Air Force Office of Scientific Research (AFOSR) under grants FA9550-09-1-0233 and FA9550-05-1-0180.

#183035 - $15.00 USD Received 8 Jan 2013; revised 1 Mar 2013; accepted 1 Mar 2013; published 16 Apr 2013